

# Reciprocity Calibration for Massive MIMO: Proposal, Modeling and Validation

Joao Vieira, Fredrik Rusek, Ove Edfors, Steffen Malkowsky, Liang Liu, Fredrik Tufvesson  
 Dept. of Electrical and Information Technology, Lund University, Sweden  
 firstname.lastname@eit.lth.se

**Abstract**—This paper presents a mutual coupling based calibration method for time-division-duplex massive MIMO systems, which enables downlink precoding based on uplink channel estimates. The entire calibration procedure is carried out solely at the base station (BS) side by sounding all BS antenna pairs. An Expectation-Maximization (EM) algorithm is derived, which processes the measured channels in order to estimate calibration coefficients. The EM algorithm outperforms current state-of-the-art narrow-band calibration schemes in a mean squared error (MSE) sense. Like its predecessors, the EM algorithm is general in the sense that it is not only suitable to calibrate a co-located massive MIMO BS, but also suitable for calibrating multiple BSs in distributed MIMO systems.

The proposed method is validated with experimental evidence obtained from a massive MIMO testbed. In addition, we address the estimated narrow-band calibration coefficients as a stochastic process across frequency, and study the subspace of this process based on measurement data. With the insights of this study, we propose an estimator which exploits the structure of the process in order to reduce the calibration error across frequency. A model for the calibration error is also proposed based on the asymptotic properties of the estimator, and is validated with measurement results.

**Index Terms**—Massive MIMO, reciprocity calibration, mutual coupling, Expectation Maximization, validation, calibration error.

## I. INTRODUCTION

MASSIVE Multiple-input Multiple-output (massive MIMO) is an emerging technology with the potential to be included in next generation wireless systems, such as fifth-generation (5G) cellular systems. Massive MIMO departs from traditional Multi-User MIMO (MU-MIMO) approaches by operating with a large number of base station (BS) antennas, typically in the order of hundreds or even thousands, to serve a relatively small number of mobile stations (MSs) [1]. Such a system setup results in a multitude of BS antennas that can be used in an advantageous manner from multiple points of view [2].

One major challenge of operating with a large number of BS antennas is that it renders explicit channel estimation in the downlink impractical. Basically, the overhead of channel estimation in the downlink and feeding back the channel estimate to the BS, scales linearly with the number of BS antennas, and quickly becomes unsupportable in mobile time-varying channels [3]. To deal with this challenge, the approach adopted is to operate in time-division-duplex (TDD) mode, rely on channel reciprocity, and use uplink channel state information (CSI) for downlink precoding purposes [4]. However, the presence of the analog front-end circuitry in practical radio units complicates the situation and makes

the baseband-to-baseband channel non-reciprocal. Explained briefly, the baseband representation of the received signals [5] experience channels that are not only determined by the propagation conditions, but also by the transceiver front-ends at both sides of the radio link. While it is generally agreed that the propagation channel is reciprocal [6], the transceiver radio frequency (RF) chains at both ends of the link are generally not [7]. Hence, in order to make use of the reciprocity assumption and rely on the uplink CSI to compute precoding coefficients, the non-reciprocal transceiver responses need to be calibrated. Such a procedure is often termed reciprocity calibration, and contains two steps: (i) estimation of calibration coefficients, and (ii) compensation by applying those to the uplink channel estimates.<sup>1</sup>

Reciprocity calibration of small scale TDD MIMO channels has been a matter of study in recent years. Depending on the system setup and requirements, the approach adopted can take many forms. For example, [7] proposed a methodology based on bi-directional measurements between the two ends of a MIMO link to estimate suitable reciprocity calibration coefficients. This calibration approach falls in the class of "over-the-air" (OTA) calibration schemes where users are involved in the calibration process. A different approach is to rely on dedicated hardware circuitry for calibration purposes, see [8]–[10]. This allows the whole calibration process to occur only at one side of the link, but can only be employed if this functionality is compatible with the hardware design of the system. Despite the possibilities of extending both mentioned calibration approaches to a massive MIMO context, e.g. [11], [12], recent calibration works suggest this is more difficult than previously thought. For example, [13] questions the feasibility of having dedicated circuits for calibration when the number of transceivers to be calibrated grows large, and [14] argues that the calibration protocols should preferably not rely on mobile units. It thus appears that an increasing trend in massive MIMO systems is to carry out the calibration entirely at the BS side only through "over-the-air" measurements.

The first proposal in this vein was presented in [15].<sup>2</sup> The work proposes an estimator for the calibration coefficients, which only makes use of channel measurements between BS antennas. More specifically, bi-directional channel measurements between a given BS antenna, so-called reference antenna, and all other antennas. This estimator was later

<sup>1</sup> However, with the term reciprocity calibration, we will interchangeably refer to the estimation step, compensation step, or both. The context will, hopefully, make clear which of the previous cases is being addressed.

<sup>2</sup>For the sake of merit, we note that [16] already suggested very similar calibration concepts but for small scale MIMO systems.

generalized in order to calibrate large-scale distributed MIMO networks [14], [17]. The estimation problem is formulated as constrained least-squares (LS) problem where the objective function uses channel measurements from a set of arbitrary antenna pairs of the network. The generality of this approach spurred many publications dealing with particular cases. For example, [18] breaks the entire estimation problem into a divide-and-conquer approach to allow calibration of multiple large arrays with low resource and computational overhead, and [19] analyzes the feasibility of the estimator to calibrate a co-located massive MIMO array based on antenna coupling. Parallel work in mutual coupling based calibration was also conducted in [13]. An estimator for the calibration coefficients, which enables maximum ratio precoding, was proposed for BS antenna arrays with very special properties.

Although it has been demonstrated that OTA reciprocity calibration only involving the BS side is feasible, some matters need further investigation. Firstly, the approaches available in the literature for co-located BSs are not of great practical convenience. They either rely on antenna elements that need to be (carefully) placed in front of the BS antenna array solely for calibration purposes [15], or are only available for a very restrictive case of antenna arrays [13]. Secondly, most estimation approaches for calibration have been derived from empirical standpoints, e.g. [13], [15], and respective extensions, e.g., [17]–[19]. It is not clear how far from fundamental estimation performance bounds, or how close to Maximum likelihood (ML) performance, such estimators are. Thus, it is of interest to conduct such analysis and infer whether there is room for improvement. If that is the case, new estimators should be studied. Thirdly, most available calibration approaches are proposed for narrow-band systems. Such systems bandwidths are usually defined by the frequency selectivity of the propagation channel, which is typically much smaller than the frequency selectivity of the transceiver responses. This results in similar calibration coefficients for adjacent frequency bands. Thus, it is of interest to model the statistical dependency of such calibration coefficients, and provide means to exploit this dependency in order to reduce the calibration error across frequency. Lastly, there is little publicly available work on validation of massive MIMO calibration schemes. The need for validation is high, as it helps solidifying many aspects on the whole body of research work. For example, [20] raises the question whether the channel reciprocity assumption holds when strong mutual coupling between BS antennas exist, and [21] questions if calibration assumptions similar to the ones used in this work, hold for massive MIMO arrays.

### A. Main Contributions of the Paper

Below, we summarize the main contributions of this work.

- We propose a convenient calibration method relying on mutual coupling between BS antennas to calibrate its analog front-ends. We make no assumptions other than channels due to mutual coupling being reciprocal.
- We show that the calibration coefficients can be estimated by solving a joint ML estimation problem. We provide an algorithm to compute the joint solution, which is a particular case of the EM algorithm.

- We validate our calibration method experimentally using a software-defined radio massive MIMO testbed. More specifically, we verify how the measured Error-Vector-Magnitude (EVM) of the downlink equalized symbols decreases as the calibration accuracy increases, in a setup where three closely spaced single-antenna users are spatially multiplexed by one hundred BS antennas.
- We study the statistical dependence of the narrow-band estimators of the calibration coefficients across frequency, and provide an estimator that exploits this dependence to reduce the calibration error.
- We propose a statistical model for the calibration error and partially validate this model with measured data.

### B. Notation and Paper Outline

The operators  $(\cdot)^*$ ,  $(\cdot)^T$ , and  $(\cdot)^H$  denote element-wise complex conjugate, transpose and Hermitian transpose, respectively. The element in the  $n$ th row and  $m$ th column of matrix  $\mathbf{A}$  is denoted by  $[\mathbf{A}]_{n,m}$ . Operators  $\mathbb{E}\{\cdot\}$  and  $\text{Var}\{\cdot\}$  denote expectation and variance operators, respectively.  $\text{Re}\{\cdot\}$  and  $\text{Im}\{\cdot\}$  return the real and imaginary part of their arguments. The matrix  $\mathbf{I}$  denotes the identity matrix, and  $\text{diag}\{a_1, a_2, \dots, a_M\}$  denotes an  $M \times M$  diagonal matrix with diagonal entries given by  $a_1, a_2, \dots, a_M$ . The set of the complex numbers is denoted by  $\mathbb{C}$ , and  $\setminus$  denotes the relative complement. Finally,  $\|\cdot\|$  denotes the Frobenius norm.

The remaining sections of the paper are as follows. Section II shows how downlink precoding can be performed using uplink channel estimates, and provides the analytical expression of the calibration coefficients. Section III presents the signal models. Section IV proposes an estimator and evaluates its MSE performance against a state-of-the-art estimator and the the Cramér-Rao lower bound (CRLB). Section V validates the proposed calibration method. Section VI studies several aspects of reciprocity calibration across adjacent narrow-bands, and proposes a model for the calibration error. Lastly, Section VII summarizes the key takeaways from this work.

## II. TDD RECIPROCITY SOLVED AT THE BS-SIDE

This section shows how downlink precoding can be performed using uplink channel estimates. Let  $K$  single-antenna users simultaneously transmit a pilot symbol at a particular sub-carrier of an OFDM system. Collecting the pilot symbols in the vector  $\mathbf{p} = [p_1 \cdots p_K]^T$ , the received signal by an  $M$ -antenna base station can be written as

$$\begin{aligned} \mathbf{y}_{\text{UP}} &= \mathbf{H}_{\text{UP}} \mathbf{p} + \mathbf{w} \\ &= \mathbf{R}_B \mathbf{H}_P \mathbf{T}_U \mathbf{p} + \mathbf{w}. \end{aligned} \quad (1)$$

In (1), the matrix  $\mathbf{R}_B = \text{diag}\{r_1^B, \dots, r_M^B\}$  models the hardware response of  $M$  BS receive RF chains (one RF chain per antenna), and the matrix  $\mathbf{T}_U = \text{diag}\{t_1^U, \dots, t_K^U\}$  models the hardware response of  $K$  transmit RF chains, i.e. one chain per user.  $\mathbf{H}_P$  is the propagation channel matrix,  $\mathbf{H}_{\text{UP}}$  is the, so-called, uplink radio channel, and  $\mathbf{w}$  is a vector modeling uplink noise. Under the reciprocal assumption of the propagation channel, the received downlink signal can be

written as

$$\begin{aligned} \mathbf{y}_{\text{DL}} &= \mathbf{H}_{\text{DL}} \mathbf{z}' + \mathbf{w}' \\ &= \mathbf{R}_U \mathbf{H}_P^T \mathbf{T}_B \mathbf{z}' + \mathbf{w}'. \end{aligned} \quad (2)$$

In (2), the matrix  $\mathbf{R}_U = \text{diag}\{r_1^U, \dots, r_K^U\}$  models the hardware response of the receive RF chains of the  $K$  users, and the matrix  $\mathbf{T}_B = \text{diag}\{t_1^B, \dots, t_K^B\}$  models the hardware response of  $M$  BS transmit RF chains. The entries of  $\mathbf{w}'$  model downlink noise,  $\mathbf{H}_{\text{DL}}$  is the downlink radio channel, and  $\mathbf{z}'$  is a vector with linearly precoded QAM symbols. In particular,  $\mathbf{z}' = \mathbf{P}\mathbf{x}$ , where  $\mathbf{P}$  is the precoding matrix, and the entries of  $\mathbf{x}$  contain QAM symbols.

Assume that an error free version of the uplink radio channel,  $\mathbf{H}_{\text{UP}}$ , is available at the BS. The transpose of the result of pre-multiplying  $\mathbf{H}_{\text{UP}}$  with the matrix  $\alpha \mathbf{T}_B \mathbf{R}_B^{-1}$ , where  $\alpha \in \mathbb{C} \setminus 0$ , is a matrix  $\mathbf{G}$  that, if used for precoding purposes by means of a linear filtering, is sufficient for spatially multiplexing terminals in the downlink with reduced crosstalk. This can be visualized by expanding  $\mathbf{G}$  as

$$\begin{aligned} \mathbf{G} &= ((\alpha \mathbf{T}_B \mathbf{R}_B^{-1}) \mathbf{H}_{\text{UP}})^T \\ &= \alpha \mathbf{T}_U \mathbf{H}_P^T \mathbf{T}_B \\ &= \alpha \mathbf{T}_U \mathbf{R}_U^{-1} \mathbf{H}_{\text{DL}}. \end{aligned} \quad (3)$$

From (3) we have that  $\mathbf{G}$  is effectively the *true* downlink radio channel  $\mathbf{H}_{\text{DL}}$  pre-multiplied with a diagonal matrix with unknown entries accounting for the user terminals responses  $\mathbf{T}_U \mathbf{R}_U^{-1}$ , and  $\alpha$ . The row space of  $\mathbf{G}$  is thus the same as of the downlink radio channel  $\mathbf{H}_{\text{DL}}$ . This is a sufficient condition to cancel inter-user interference if, e.g., ZF precoding is used [14].

From (3), it can also be seen that any non-zero complex scalar  $\alpha$  provides equally good calibration.<sup>3</sup> Thus, the matrix

$$\begin{aligned} \mathbf{C} &= \text{diag}\{c_1, \dots, c_M\} \\ &= \text{diag}\left\{\frac{t_1^B}{r_1^B}, \dots, \frac{t_M^B}{r_M^B}\right\} \\ &= \mathbf{T}_B \mathbf{R}_B^{-1} \end{aligned} \quad (4)$$

is the, so-called, calibration matrix, and  $\{c_m\}$  are the calibration coefficients which can be estimated up to a common complex scalar  $\alpha$ . We remark that, although not strictly necessary to build estimators, the concept of a reference transceiver [15] can be used to deal with the ambiguity of estimating  $\{c_m\}$  up to  $\alpha$ .<sup>4</sup> A thorough performance analysis on this and other calibration methodologies is found in [22].

The rest of the paper deals with estimation aspects of  $c_m = t_m^B / r_m^B$ . Thus, for notational simplicity, we write  $t_m = t_m^B$ ,  $r_m = r_m^B$ ,  $\mathbf{R} = \mathbf{R}_B$ , and  $\mathbf{T} = \mathbf{T}_B$ . Also, we stack  $\{c_m\}$  in the vector  $\mathbf{c} = [c_1 \dots c_M]^T$ , for later use.

<sup>3</sup>This follows since both magnitude and phase of  $\alpha$  are not relevant for this calibration setup. The former holds since any real scaled channel estimate provides the same precoder matrix  $\mathbf{P}$ , if the precoder has a fixed norm. The latter follows from (3), since the (phases of the) diagonal entries of  $\mathbf{T}_U \mathbf{R}_U^{-1}$  are unknown to the precoder in this calibration setup.

<sup>4</sup>Explained briefly, assuming  $c_{\text{ref}} = 1$  and solving for  $\{c_m\} \setminus c_{\text{ref}}$ , where  $c_{\text{ref}}$  is the calibration coefficient associated with the reference transceiver.

### III. SIGNAL MODELS

#### A. Inter-radio model

To estimate the calibration coefficients  $c_m$  we sound the  $M$  antennas one-by-one by transmitting a sounding signal from each one and receiving on the other  $M - 1$  silent antennas. Let the sounding signal transmitted by antenna  $m$  be  $s_m = 1 \forall m$ , unless explicitly said otherwise. Also, let  $y_{n,m}$  denote the signal received at antenna  $n$  when transmitting at antenna  $m$ . It follows that the received signals between any pair of antennas can be written as

$$\begin{bmatrix} y_{n,m} \\ y_{m,n} \end{bmatrix} = h_{n,m} \begin{bmatrix} r_n t_m & 0 \\ 0 & r_m t_n \end{bmatrix} \begin{bmatrix} s_m \\ s_n \end{bmatrix} + \begin{bmatrix} n_{n,m} \\ n_{m,n} \end{bmatrix}, \quad (5)$$

where

$$h_{n,m} = \bar{h}_{n,m} + \tilde{h}_{n,m} \quad (6)$$

$$= |\bar{h}_{n,m}| \exp(j2\pi\phi_{n,m}) + \tilde{h}_{n,m} \quad (7)$$

models the reciprocal channels between BS antennas. The first term  $\bar{h}_{n,m}$  describes a channel component due to mutual coupling between antenna elements, often stronger for closely spaced antennas, which we lay down a model for in Sec. III-B. The term  $\tilde{h}_{n,m}$ , which absorbs all other channel multipath contributions except for the mutual coupling, e.g. reflections by scatterers in front of the BS, is modeled by an i.i.d. zero-mean circularly symmetric complex Gaussian random variable with variance  $\sigma^2$ . Non-reciprocal channel components are modeled by  $r_m$  and  $t_m$  which materially map to the cascade of hardware components, mainly in the analog front-end stage of the receiver and transmitter, respectively. We assume i.i.d. circularly symmetric zero-mean complex Gaussian noise contributions  $n_{m,n}$  with variance  $N_0$ . Letting  $[\mathbf{Y}]_{m,n} = y_{m,n}$ , the received signals can be expressed more compactly as

$$\mathbf{Y} = \mathbf{RHT} + \mathbf{N}. \quad (8)$$

We note that the diagonal entries in the  $M \times M$  matrix  $\mathbf{Y}$  are undefined, and that  $\mathbf{H} = \mathbf{H}^T$  is assumed.

#### B. Modeling Mutual Coupling

The purpose of this section is to provide a model for the mutual coupling between antenna elements, i.e.  $\bar{h}_{m,n}$ , as a function of their distance. We remark that this model is used only for simulation purposes, and not to derive any of the upcoming estimators of  $\mathbf{c}$ .

1) *Test Array Description:* The antenna array considered for modelling is our 2-dimensional planar structure with dual-polarized patch elements spaced by half a wavelength. More information about the antenna array can be found in [23]. The dimensional layout of the array adopted for this work corresponds to the  $4 \times 25$  rectangular grid in the upper part of the array shown in Fig. 1. Only one antenna port is used per antenna element, and the unused ports are terminated with matching loads. For a given antenna, the polarization port is chosen such that its adjacent antennas - the antennas spaced by half wavelength, which are four at most - are cross-polarized. This setting provides, so-called, polarization diversity, and reduces mutual coupling effects between adjacent antennas since co-polarized antennas couple stronger [24].

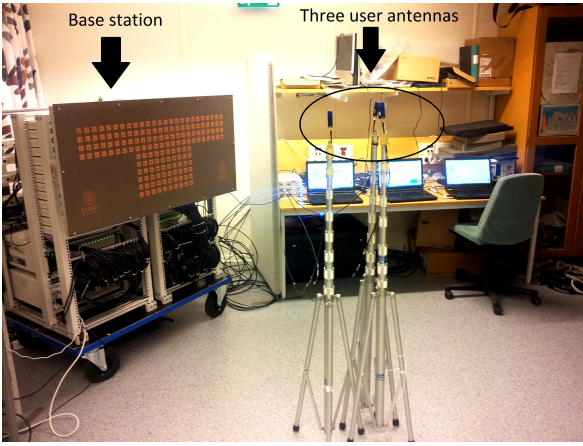


Fig. 1. The massive MIMO lab setup used throughout this work. The BS is on the left side where a "T" shaped antenna array can be seen. Three closely spaced user antennas stand the middle of the picture.

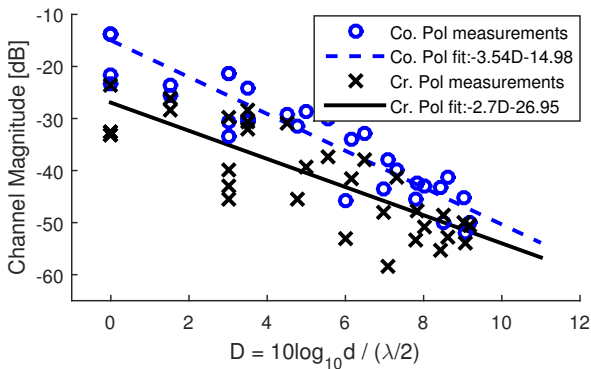


Fig. 2. Measured coupling magnitudes  $|\bar{h}_{n,m}|$  between multiple antenna pairs. The circles corresponds to measurements between co-polarized antenna elements, and the crosses to cross polarized antenna elements. The variable  $d$  corresponds to the physical distance between antenna elements. The straight lines represent the corresponding linear LS fits.

2) *Modeling coupling gains between antennas:* To model the antenna coupling, the channel magnitude  $|\bar{h}_{n,m}|$  between several pairs of cross and co-polarized antennas were measured in an anechoic chamber using a Vector Network Analyzer, at 3.7 GHz - the center frequency of the array. Fig. 2 shows the measured channel magnitudes. Different channel magnitudes for the very same measured distance and polarization cases, are due mostly to the relative orientation of the antenna pair with respect to their polarization setup. For example, vertically (co-)polarized antennas couple more strongly when they are oriented horizontally. A linear LS fit was performed to model the coupling gain  $|\bar{h}_{n,m}|$  as a function of antenna distance. The phase  $\phi_{m,n} = \phi_{n,m}$  is modeled uniformly in  $[0, 1]$ , as a clear dependence with distance was not found.

#### IV. ESTIMATION OF THE CALIBRATION COEFFICIENTS

In this section we deal with estimation aspects of the calibration coefficient matrix  $\mathbf{C} = \mathbf{TR}^{-1}$ . We introduce the state-of-art estimator of  $\mathbf{C}$  [14], [17], and propose an ML estimator. Finally, we compute the CRLB, and conclude with a performance analysis by means of Monte Carlo computations.

##### A. The Generalized Method of Moments estimator

Based on the structure of (8), [14] and [17] identified that

$$\mathbb{E}\{y_{n,m}c_m - y_{m,n}c_n\} = 0. \quad (9)$$

Define  $g_{m,n} = y_{n,m}c_m - y_{m,n}c_n$ , and  $\mathbf{g}(\mathbf{c}) = [g_{1,2} \dots g_{1,M} g_{2,3} \dots g_{2,M} \dots g_{M-1,M}]^T$ .<sup>5</sup> An estimator for  $\mathbf{c}$  was proposed by solving

$$\hat{\mathbf{c}}_{\text{GMM}} = \arg \min_{\mathbf{c}} \mathbf{g}^H(\mathbf{c})\mathbf{W}\mathbf{g}(\mathbf{c}) \quad (10)$$

*s.t.*  $f_c(\mathbf{c})=1$

with  $\mathbf{W} = \mathbf{I}$ . Various constraints  $f_c(\mathbf{c}) = 1$  were suggested to avoid the all-zero solution. By setting the gradient with respect to  $\mathbf{c}$  to zero, an estimator in closed-form was given. Next, we provide a few remarks on this approach.

A fact not identified in [14] and [17], is that this estimator is an instance of a estimation framework widely used for statistical inference in econometrics, namely the generalized method of moments (GMM). The function  $g_{m,n}$  - whose expectation is zero - is termed a moment condition within the GMM literature [25]. On a different note, with a proper setting of the weighting matrix  $\mathbf{W}$ , it can be shown that the solution to (10) provides an estimator that is asymptotically efficient [25]. However, no such claim can be made in the low SNR regime, where an optimal form of  $\mathbf{W}$  is not available in the literature. It thus appears that an inherent problem of the GMM estimator is the selection of the weighting matrix  $\mathbf{W}$ . Nevertheless, it provides an estimator based on a cost function formulation where nuisance parameters for calibration, as  $h_{m,n}$ , are conveniently left out.

##### B. Joint Maximum-Likelihood estimation

Here we address joint maximum likelihood estimation for  $\mathbf{c}$  and for the equivalent channel  $\Psi = \mathbf{RHR}$ . Noting that (8) can be written as

$$\begin{aligned} \mathbf{Y} &= \mathbf{RHRC} + \mathbf{N} \\ &= \Psi\mathbf{C} + \mathbf{N}, \end{aligned} \quad (11)$$

the optimization problem is

$$\begin{aligned} [\hat{\mathbf{c}}, \hat{\Psi}] &= \arg \max_{\mathbf{c}, \Psi} p(\mathbf{Y}|\mathbf{C}, \Psi) \\ &= \arg \min_{\mathbf{c}, \Psi} \|\mathbf{Y} - \Psi\mathbf{C}\|^2, \end{aligned} \quad (12)$$

where  $p(\mathbf{Y}|\mathbf{C}, \Psi)$  denotes the probability density function of  $\mathbf{Y}$  conditioned on  $\mathbf{C}$  and  $\Psi$ . We note that a vectorized version of (11) can be written as

$$\tilde{\mathbf{Y}} = \Psi_{\text{eq}}(\tilde{\Psi})\mathbf{c} + \tilde{\mathbf{N}}, \quad (13)$$

or as

$$\tilde{\mathbf{Y}} = \mathbf{C}_{\text{eq}}(\mathbf{c})\tilde{\Psi} + \tilde{\mathbf{N}}, \quad (14)$$

where  $\tilde{\Psi}$  stacks all  $\psi_{n,m} = [\Psi]_{n,m}$  into an  $(M^2 - M)/2 \times 1$  vector, and  $\Psi_{\text{eq}}(\tilde{\Psi})$  and  $\mathbf{C}_{\text{eq}}(\mathbf{c})$  are equivalent observation matrices which are constructed from  $\tilde{\Psi}$  and  $\mathbf{c}$ , respectively. The particular structures of these matrices are implicitly defined from (13) and (14), but it can be pointed out that with

<sup>5</sup>The dependency of  $\mathbf{g}(\mathbf{c})$  on  $y_{n,m}$  is explicitly left out, for notation convenience.

proper structuring, these matrices can be written as block diagonal matrices, where each block is a column vector.

From (14), it is seen that for a given  $\mathbf{C}_{\text{eq}}(\mathbf{c})$ , the ML estimator of  $\tilde{\Psi}$  is given by

$$\tilde{\Psi}_{\text{ML}} = \mathbf{C}_{\text{eq}}^\dagger(\mathbf{c})\tilde{\mathbf{Y}}, \quad (15)$$

where  $\mathbf{C}_{\text{eq}}^\dagger(\mathbf{c})$  is the Moore-Penrose pseudo-inverse of  $\mathbf{C}_{\text{eq}}(\mathbf{c})$ . If in (14), we replace  $\tilde{\Psi}$  by its ML estimate  $\tilde{\Psi}_{\text{ML}}$ , it follows that the ML solution for  $\mathbf{c}$  is

$$\hat{\mathbf{c}}_{\text{ML}} = \arg \min_{\mathbf{c}} \|\tilde{\mathbf{Y}} - \mathbf{C}_{\text{eq}}(\mathbf{c})\mathbf{C}_{\text{eq}}^\dagger(\mathbf{c})\tilde{\mathbf{Y}}\|^2. \quad (16)$$

By leaving out the terms that do not depend on  $\mathbf{c}$ , (16) can be written as

$$\hat{\mathbf{c}}_{\text{ML}} = \arg \max_{\mathbf{c}} J_{\text{ML}}(\mathbf{c}), \quad (17)$$

where  $J_{\text{ML}}(\mathbf{c}) = \tilde{\mathbf{Y}}^H \mathbf{C}_{\text{eq}}(\mathbf{c})\mathbf{C}_{\text{eq}}^\dagger(\mathbf{c})\tilde{\mathbf{Y}}$ . The solution to (17) is not unique since  $J_{\text{ML}}(\mathbf{c})$  is an homogenous function of degree 0. Unfortunately, it appears that none of such solutions can be found in closed-form. We have implemented the conjugate gradient method in a Fletcher-Reeves setting with an optimized step-size through a line-search. However, this approach turns out to be far less robust than, and computationally inferior to, the method provided in the next section. Therefore we omit to provide the gradient in closed form.

### C. An EM Algorithm to find the joint ML Estimate

Here we provide a robust and computational efficient algorithm to find the joint ML estimate of  $\mathbf{c}$  and  $\Psi$ . Instead of pursuing an approach similar to the one used to reach (17), the algorithm has its roots in the joint ML solution, found by setting the gradient of  $\|\mathbf{Y} - \Psi\mathbf{C}\|^2$  to zero. Before presenting the algorithm, we therefore briefly address this gradient approach.

Each entry of (11) is given by  $y_{n,m} = \psi_{n,m}c_m + n_{n,m}$ . The first derivative of  $\|\mathbf{Y} - \Psi\mathbf{C}\|^2$  with respect to  $c_m^*$  is given by

$$\begin{aligned} \frac{\partial \|\mathbf{Y} - \Psi\mathbf{C}\|^2}{\partial c_m^*} &= \frac{\partial}{\partial c_m^*} \sum_{m=1}^M \sum_{\substack{n=1 \\ n \neq m}}^M |y_{n,m} - \psi_{n,m}c_m|^2 \\ &= \sum_{\substack{n=1 \\ n \neq m}}^M -y_{n,m}\psi_{n,m}^* - |\psi_{n,m}|^2 c_m. \end{aligned} \quad (18)$$

Setting (18) to zero and solving for  $c_m$  yields

$$c_m = \frac{\sum_{\substack{n=1 \\ n \neq m}}^M y_{n,m}\psi_{n,m}^*}{\sum_{\substack{n=1 \\ n \neq m}}^M |\psi_{n,m}|^2}, \quad (19)$$

which can be expressed in a vector form as

$$\mathbf{c} = \Psi_{\text{eq}}^\dagger(\tilde{\Psi})\tilde{\mathbf{Y}}. \quad (20)$$

In a similar fashion, setting the first derivative of  $\|\mathbf{Y} - \Psi\mathbf{C}\|^2$  with respect to  $\psi_{n,m}^*$  to zero and solving for  $\psi_{n,m}$  provides

$$\psi_{n,m} = \frac{y_{n,m}c_m^* + y_{n,m}c_m^*}{|c_n|^2 + |c_m|^2} \quad (21)$$

---

### Algorithm 1 Expectation-Maximization

---

**Require:** Measurement matrix  $\mathbf{Y}$ , convergence threshold  $\Delta_{\text{ML}}$ , regularization constant  $\epsilon$ , initial guess for coefficients  $\hat{\mathbf{c}}$

- 1: **Initialization:** set  $\Delta = \delta$  where  $\delta > \Delta_{\text{ML}}$
- 2: **while**  $\Delta \geq \Delta_{\text{ML}}$  **do**
- 3:   Build  $\mathbf{C}_{\text{eq}}(\hat{\mathbf{c}})$
- 4:    $\tilde{\Psi}_{\text{ML}} = \left( \mathbf{C}_{\text{eq}}^H(\hat{\mathbf{c}})\mathbf{C}_{\text{eq}}(\hat{\mathbf{c}}) + \epsilon \mathbf{I} \right)^{-1} \mathbf{C}_{\text{eq}}^H(\hat{\mathbf{c}})\tilde{\mathbf{Y}}$
- 5:   Build  $\Psi_{\text{eq}}(\tilde{\Psi}_{\text{ML}})$
- 6:    $\hat{\mathbf{c}}_{\text{ML}} = \left( \Psi_{\text{eq}}^H(\tilde{\Psi}_{\text{ML}})\Psi_{\text{eq}}(\tilde{\Psi}_{\text{ML}}) + \epsilon \mathbf{I} \right)^{-1} \Psi_{\text{eq}}^H(\tilde{\Psi}_{\text{ML}})\tilde{\mathbf{Y}}$
- 7:    $\Delta = J_{\text{ML}}(\hat{\mathbf{c}}_{\text{ML}}) - J_{\text{ML}}(\hat{\mathbf{c}})$
- 8:    $\hat{\mathbf{c}} = \hat{\mathbf{c}}_{\text{ML}}$
- 9: **end while**

**Output:** Calibration coefficients estimate  $\hat{\mathbf{c}}_{\text{ML}}$

---

which can be expressed in a vector form as (15). Combining the results from (20) and (15) yield the joint ML solution

$$\begin{bmatrix} \hat{\mathbf{c}}_{\text{ML}} \\ \tilde{\Psi}_{\text{ML}} \end{bmatrix} = \begin{bmatrix} \Psi_{\text{eq}}^\dagger(\tilde{\Psi}_{\text{ML}}) \\ \mathbf{C}_{\text{eq}}^\dagger(\hat{\mathbf{c}}_{\text{ML}}) \end{bmatrix} \tilde{\mathbf{Y}}. \quad (22)$$

The literature on numerical methods to solve systems of the nature of (22) is vast [26]. However, the particular structure of (22) suggests that a more pragmatic approach can be pursued. More specifically, (22) can be separated into two sub-problems, i.e., solving for  $\hat{\mathbf{c}}_{\text{ML}}$  and  $\tilde{\Psi}_{\text{ML}}$  separately. Since each of the solutions depend on previous estimates, the joint solution can be computed iteratively, by sequentially solving two separate LS problems, given an initial guess. Since each iteration estimates  $\mathbf{c}$  and  $\tilde{\Psi}$  separately, this approach is, in fact, a particular case of the EM algorithm [27], where only the first moment of the nuisance parameters  $\{\psi_{m,n}\}$  is estimated. The convergence can be addressed by evaluating  $J_{\text{ML}}(\cdot)$  with consecutive estimates as input. For sake of clarity, Algorithm 1 summarizes the iteration procedure we propose to solve (12). The GMM or other estimators - as the one in [15] - can be used to produce an initial guess. Note that we introduced a regularization constant  $\epsilon$ , but unless explicitly said otherwise, we assume  $\epsilon = 0$ .

We highlight that the calibration coefficients  $\mathbf{c}$  and the matrix  $\Psi$  are jointly estimated. This results in a robust estimator since the (strength of the) equivalent channels  $\psi_{m,n}$  are inherently used by the estimator. This feature makes the ML estimator very suitable to calibrate distributed (massive) MIMO systems, where channel fading often occurs [14]. As pointed out in Sec. IV-A, such feature is not available in (10).

### D. Complexity of the EM algorithm

The complexity of each iteration of Algorithm 1 is dominated by steps 4 and 6, as many computations in steps 7 can be reused from step 4. From (21), each  $\psi_{m,n}$  requires a few multiplications and additions. Since  $(M^2 - M)/2$  such calculations are need to be performed to compute (15), the complexity order of Step 4 is  $\mathcal{O}(M^2)$ . Similarly, the complexity of step 6 is  $\mathcal{O}(M^2)$  which can be seen from (19). Explained briefly, the complexity of each calibration coefficient  $c_m$  is  $\mathcal{O}(M)$ , and  $M$  such calibration coefficients need to be computed. Overall, each iteration of the EM algorithm is of complexity  $\mathcal{O}(M^2)$ , and the algorithm's complexity is  $\mathcal{O}(N_{\text{ite}} M^2)$ , with  $N_{\text{ite}}$  being the number of iterations needed for convergence.

It can already be mentioned that - as seen in Sec. IV-G4 - a proper choice of  $\epsilon$  makes  $N_{\text{ite}} \ll M$ .

As for the GMM estimator, the closed-form solutions presented in [14] and [17] have complexity orders of  $\mathcal{O}(M^3)$ , as they consist of an inversion of a Hermitian matrix of size  $M-1$ , and finding the eigenvector associated with the smallest eigenvalue of a Hermitian matrix of size  $M$ .

### E. Interlude: Closed-form ML calibration of Linear Arrays

Here we present a special case when (17) can be solved in closed-form. Consider an  $M$ -antenna linear array, and let  $m$  index the antennas in ascending order starting at one edge of the linear array. Assume that mutual coupling only exists between adjacent antenna elements, and that the channel between any other antenna pairs is weak enough so that it can be neglected without any noticeable impact on performance. With  $\mathbf{y}_{n,m} = [y_{n,m} \ y_{m,n}]^T$ , it follows that (17) can be written as

$$\{\hat{c}_m\} = \arg \max_{\{c_m\}} \sum_{\ell=1}^{M-1} f_L(c_\ell, c_{\ell+1}, \mathbf{y}_{\ell+1,\ell}), \quad (23)$$

where  $f_L(c_\ell, c_{\ell+1}, \mathbf{y}_{\ell+1,\ell})$  is defined as

$$\frac{\mathbf{y}_{\ell+1,\ell}^H \begin{bmatrix} c_\ell \\ c_{\ell+1} \end{bmatrix} [c_\ell^* \ c_{\ell+1}^*] \mathbf{y}_{\ell+1,\ell}}{|c_\ell|^2 + |c_{\ell+1}|^2}. \quad (24)$$

Our ability to solve (23) is due to the following property.

*Property 1:* For the function  $f_L(c_\ell, c_{\ell+1}, \mathbf{y}_{\ell+1,\ell})$ , the maximum over  $c_{\ell+1}$  equals  $\|\mathbf{y}_{\ell+1,\ell}\|^2$ , and thus it does not depend on  $c_\ell$ .

Hence, the ML estimate of  $c_{\ell+1}$ , i.e.  $\hat{c}_{\ell+1}$ , can be found if  $c_\ell$  is assumed to be known. With that, the joint maximization problem (23) can be split into

$$\hat{c}_{\ell+1} = \arg \max_x f_L(\hat{c}_\ell, x, \mathbf{y}_{\ell+1,\ell}).$$

This optimization is straightforward and the solution is

$$\hat{c}_{\ell+1} = \hat{c}_\ell \frac{y_{\ell+1,\ell}^* y_{\ell,\ell+1}}{|y_{\ell+1,\ell}|^2}. \quad (25)$$

Using a reference antenna as a starting point, e.g.  $c_1 = 1$ , the solution for any  $c_m$ , with  $m > 1$ , can be obtained from (25) in a sequential manner. Noticeably, it can be shown that for this special case, (25) coincides with the GMM estimate (10).

### F. The Cramér-Rao Lower Bound

In this section we compute the CRLB [27], for the calibration coefficients  $\{c_m\} \setminus c_{\text{ref}}$ .<sup>6</sup> This is achieved by assuming  $t_{\text{ref}} = r_{\text{ref}} = 1$ , and treating  $c_{\text{ref}} = t_{\text{ref}}/r_{\text{ref}}$  as known for estimation purposes. Define the  $(4M-4) \times 1$  vector of real parameters

$$\boldsymbol{\theta} = [\text{Re}\{t_1\} \ \text{Im}\{t_1\} \ \text{Re}\{r_1\} \ \text{Im}\{r_1\} \ \text{Re}\{t_2\} \ \dots \ \text{Im}\{r_M\}]^T, \quad (26)$$

where  $t_{\text{ref}}$  and  $r_{\text{ref}}$  do not enter. The CRLB for  $\{c_m\} \setminus c_{\text{ref}}$  is given by the diagonal entries of the transformed Fisher information matrix [27]

$$\text{var}(\hat{c}_m) \geq \left[ \frac{q(\boldsymbol{\theta})}{\partial \boldsymbol{\theta}} \mathbf{I}^{-1}(\boldsymbol{\theta}) \frac{q(\boldsymbol{\theta})}{\partial \boldsymbol{\theta}} \right]_{m,m}^H, \quad m \neq \text{ref}, \quad (27)$$

where  $\mathbf{I}(\boldsymbol{\theta})$  is the Fisher information matrix of  $\boldsymbol{\theta}$ . The transformation of  $\boldsymbol{\theta}$  into the calibration coefficients is given by

$$q(\boldsymbol{\theta}) = \left[ \frac{\text{Re}\{t_1\} + j \text{Im}\{t_1\}}{\text{Re}\{r_1\} + j \text{Im}\{r_1\}} \ \dots \ \frac{\text{Re}\{t_M\} + j \text{Im}\{t_M\}}{\text{Re}\{r_M\} + j \text{Im}\{r_M\}} \right]^T.$$

Next we address the Fisher information matrix  $\mathbf{I}(\boldsymbol{\theta})$ . Assuming that the mean of the observation pair  $\mathbf{y}_{n,m}$  is at hand<sup>7</sup> and is given by

$$\boldsymbol{\mu}_{n,m} = \mathbb{E}\{\mathbf{y}_{n,m}\} = \bar{h}_{n,m} [r_n t_m \ r_m t_n]^T, \quad (28)$$

it follows that the covariance matrix of  $\mathbf{y}_{n,m}$  is

$$\begin{aligned} \boldsymbol{\Sigma}_{n,m} &= \text{Var}\{\mathbf{y}_{n,m} \mathbf{y}_{n,m}^H\} \\ &= \begin{bmatrix} |r_n|^2 |t_m|^2 \sigma^2 + N_0 & r_n t_m r_m^* t_n^* \sigma^2 \\ r_m t_n r_n^* t_m^* \sigma^2 & |r_m|^2 |t_n|^2 \sigma^2 + N_0 \end{bmatrix}. \end{aligned} \quad (29)$$

We can observe that the PDF of  $\mathbf{Y}'$ , where

$$\mathbf{Y}' = [\mathbf{y}_{1,2}^T \ \dots \ \mathbf{y}_{1,M}^T \ \mathbf{y}_{2,3}^T \ \dots \ \mathbf{y}_{2,M}^T \ \dots \ \mathbf{y}_{M-1,M}^T]^T,$$

conditioned on  $\boldsymbol{\theta}$ , follows a multivariate Gaussian distribution, i.e.,  $p(\mathbf{Y}'|\boldsymbol{\theta}) \sim \mathcal{CN}(\boldsymbol{\mu}, \boldsymbol{\Sigma})$ , with mean  $\boldsymbol{\mu} = [\boldsymbol{\mu}_{1,2}^T \ \dots \ \boldsymbol{\mu}_{1,M}^T \ \boldsymbol{\mu}_{2,3}^T \ \dots \ \boldsymbol{\mu}_{2,M}^T \ \dots \ \boldsymbol{\mu}_{M-1,M}^T]^T$  and block diagonal covariance

$$\boldsymbol{\Sigma} = \text{diag}\{\boldsymbol{\Sigma}_{1,2}, \dots, \boldsymbol{\Sigma}_{1,M}, \boldsymbol{\Sigma}_{2,3}, \dots, \boldsymbol{\Sigma}_{2,M}, \dots, \boldsymbol{\Sigma}_{M-1,M}\}. \quad (30)$$

With that, we have

$$[\mathbf{I}(\boldsymbol{\theta})]_{i,j} = \text{Tr} \left\{ \boldsymbol{\Sigma}^{-1} \frac{\partial \boldsymbol{\Sigma}}{\partial \theta_i} \boldsymbol{\Sigma}^{-1} \frac{\partial \boldsymbol{\Sigma}}{\partial \theta_j} \right\} + 2 \text{Re} \left\{ \frac{\partial \boldsymbol{\mu}^H}{\partial \theta_i} \boldsymbol{\Sigma}^{-1} \frac{\partial \boldsymbol{\mu}}{\partial \theta_j} \right\}, \quad (31)$$

with  $1 \leq i \leq (4M-4)$  and  $1 \leq j \leq (4M-4)$ . The remaining computations of  $[\mathbf{I}(\boldsymbol{\theta})]_{i,j}$  are straightforward and thus omitted. To finalize, we note that without the convention of  $t_{\text{ref}} = r_{\text{ref}} = 1$ , and thus  $\boldsymbol{\theta}$  is a  $4M \times 1$  vector instead, the map  $\boldsymbol{\theta} \mapsto \boldsymbol{\mu}$  is not injective which renders  $\mathbf{I}(\boldsymbol{\theta})$  not invertible.

### G. Performance Assessment

1) *MSE as the performance metric:* There are several ways of assessing the goodness of an estimator for the calibration coefficients. In the light of the targeted application, a bottom line measure is achieved sum-rates or similar. Such measures are, however, analytically challenging specially if a (tight) performance bound is to be derived. As the calibration is, for the most part, an estimation problem, a natural way to assess performance is through the MSE of the estimator [27]. This also allows the estimation performance to be bounded by the CRLB. For these reasons the upcoming analysis focus on the MSE of the calibration coefficients.

<sup>7</sup>This assumption is only used for the CLRb computations, as it is not used to derive any of the aforementioned estimators. The implications of this assumption are discussed in Sec. IV-G3.

<sup>6</sup>The exclusion of  $c_{\text{ref}}$  is justified in the end of this subsection.

For consistency with the reference antenna concept used in the CRLB computations, the MSE of the EM algorithm output, i.e.,  $\hat{c}_{ML}$ , is defined as

$$\text{MSE}_m = \text{E} \left\{ |c_m - [\hat{c}_{ML}]_{m,1} / [\hat{c}_{ML}]_{ref,1}|^2 \right\}, \quad (32)$$

since the estimated "reference" coefficient  $[\hat{c}_{ML}]_{ref,1}$  is not necessarily equal to 1. This is because the concept of reference antenna is not used during the derivations of the EM algorithm. As for the GMM estimator, the constraint provided in [17] is adopted, i.e.,  $c_{ref} = 1$  in (10), which is already coherent with the CRLB computed.

2) *Simulation setup*: We simulate reciprocity calibration over a  $4 \times 25$  rectangular array as the one in Fig.1. The linear regression parameters obtained in Sec. III-B2 are used to model the coupling gains  $\bar{h}_{m,n}$ . The  $m$ th transceiver maps to the antenna in row  $a_{row}$  and column  $a_{col}$  of the array as  $m = 25(a_{row} - 1) + a_{col}$ . The reference transceiver index is set to  $ref = 38$ , as it is associated with one of the most central antenna elements of the 2-dimensional array.

The transmitter  $t_m$  and receiver  $r_m$  gains are set to  $t_m = (0.9 + \frac{0.2m}{M} \exp(-j2\pi m/M))/t_{ref}$  and  $r_m = (0.9 + \frac{0.2M-m}{M} \exp(j2\pi m/M))/r_{ref}$ , respectively. We used this deterministic setting for the transceivers, due to simplicity, as a statistical model for  $t_m$  and  $r_m$  is not at hand. Moreover, this deterministic setting incorporates eventual mismatches within the transceivers complex amplitude, and allows for a direct comparison of the estimators' MSE with the CRLB.

The variance  $\sigma^2$  of the multipath propagation contribution during calibration is set to  $-60$  dB. Our motivation for this value is as follows. If the closest physical scatterer to the BS is situated, say, 15 meters away, then by Friis' law [28] we have a path loss of around  $10 \log_{10}(\frac{4\pi d}{\lambda}) = 10 \log_{10}(\frac{4\pi(2 \times 15m)}{3 \times 10^8/(3.7 \times 10^9)}) = 73$  dB per path. This number does not account for further losses due to reflections and scattering. Based on this, we use  $-60$  dB as the power (variance) of the resulting channel stemming from a large number of such uncorrelated paths.

For the upcoming analysis, we note that the GMM estimator is used to produce the initial guess for the EM algorithm.

3) *Estimators' MSE vs CRLB*: Fig. 3 compares the MSE of the estimators with the CRLB (solid line) for two transceiver cases. Both estimators appear to be asymptotically efficient. Noticeably, the performance of the EM algorithm is grossly superior to the GMM at low SNR, i.e. around 10 dB in some regions. This is mainly because the GMM estimator does not appropriately weight moment conditions with less quality. This effect is inherently compensated in the EM algorithm, as pointed out in Sec. IV-C.

Two remarks about the CRLB itself is now in place. Firstly, the assumptions used during its computations, i.e. that  $\bar{h}_{m,n}$ ,  $N_0$  and  $\sigma^2$  are known for estimation purposes, could result in an underestimated CRLB. This is because none of the estimators studied have these parameters available during estimation of  $c$ . Indeed, the results in Fig. 3 suggest that the assumptions used during the CRLB computations do not affect the final CRLB value as the estimators' MSE asymptotically converges to the computed CRLB. This is convenient since (asymptotically) efficient estimators can still be built with limited information. Secondly, it was assumed that  $\phi_{m,n}$  - the

phase of  $\bar{h}_{m,n}$  - is known during the CRLB computations, although it is originally modeled as a random variable in Sec.III-B2. However, if  $\phi_{m,n}$  is assumed to be known, the CRLB is independent of the current realization of  $\phi_{m,n}$ . This is because a phase rotation in  $\mu_{n,m}$ , does not influence (31), due to the structure of  $\Sigma^{-1}$ .

4) *Convergence of the EM algorithm*: Fig. 4 illustrates the MSE of the EM algorithm across iterations, and the role played by the regularization constant  $\epsilon$ . The MSE at the 0th iteration and the MSE obtained after convergence match the results of Fig. 3 when  $1/N_0 = 40$  dB, namely the MSE of the GMM estimator and the MSE of the EM algorithm, respectively. Overall, the higher  $\epsilon$ , the faster the convergence. The results also suggests that proper choice of  $\epsilon$  provides MSE gains compared to the unregularized case, and thus can potentially yield a lower MSE than the CRLB. Notice that this does not conflict with the CRLB theorem, as an estimator built with  $\epsilon \neq 0$  is not necessarily unbiased.

One iteration of the EM-algorithm can be seen as a fixed point iteration. This is because one iteration takes  $\hat{c}$  in step 3 as input, and provides  $\hat{c}$  in step 8 as output. Our simulations indicate that the Lipschitz constant of such map is smaller than one, for any regularized case of Fig. 4. This property suggests that the map can be made contractive, and therefore convergence to the unique fixed-point is guaranteed. Hence, regularization not only reduces the number of iterations, but can also make the convergence point independent of the starting position (therefore the GMM estimate needs not to be used as a starting point). If ML estimation is still to be pursued, the convergence can be accelerated by setting  $\epsilon \neq 0$  in the initial iterations. To finalize, we note that the same scaled identity matrix was used for regularization in steps 4 and 6 of Algorithm 1, as a matter of simplicity. Parameter tuning for the entries of both regularization matrices is left as future work.

#### H. Calibration with Reduced Measurement Sets

It might be beneficial to work with a reduced measurement set, by only relying on high quality measurements. This is possible as long as (11) is not under-determined. The dashed line in Fig. 3 shows the CRLB when a reduced measurements set, comprising the measurements between antenna pairs whose elements are distanced by at most  $\sqrt{2}$  wavelengths, is used. The number of measurement signals in this case drops from  $M(M-1)$  to less than  $8M$ , since one antenna signals to, at most, 8 other antennas. The performance loss turns out not to be significant, i.e. 2 dB for the neighbor case and 4 dB for the edge case, considering the number of signals discarded. This indicates that the channels between neighbor antennas - which are dominated by mutual coupling - are the most important channels for calibration. Also, closed-form estimators may also be possible when using reduced measurement sets, as in Sec. IV-E. Another main benefit of using reduced measurement sets is the reduction of system overhead dedicated for calibration. One such example setup, is if different antenna pairs are situated in such a way that their channels can be sounded simultaneously with low interference.

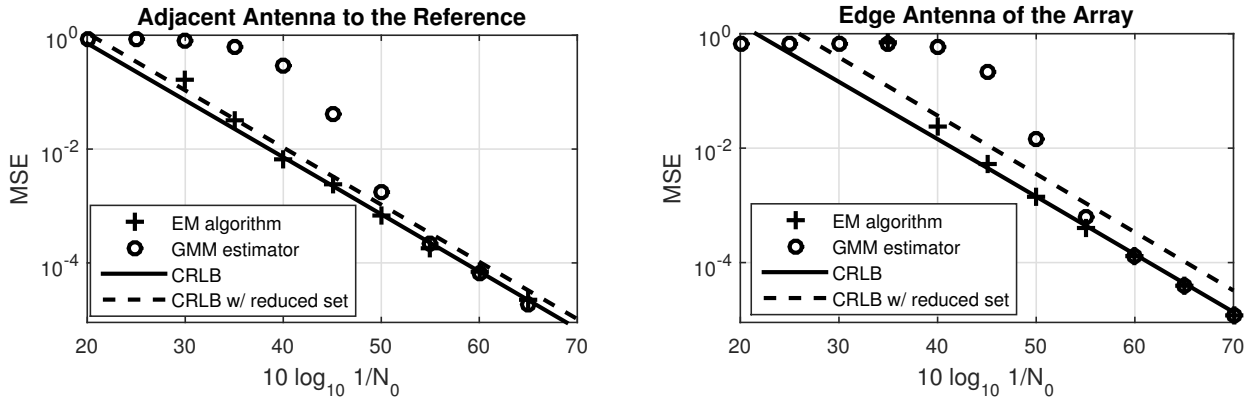


Fig. 3. MSE of the GMM estimator and the EM algorithm, versus their CRLB (solid line), for 2 extreme transceiver cases. Namely, a transceiver associated with an antenna at the edge of the array, and a transceiver associated with an antenna adjacent to the reference. The CRLB plotted by a dashed line is discussed in Sec. IV-H, but is shown here for convenience.

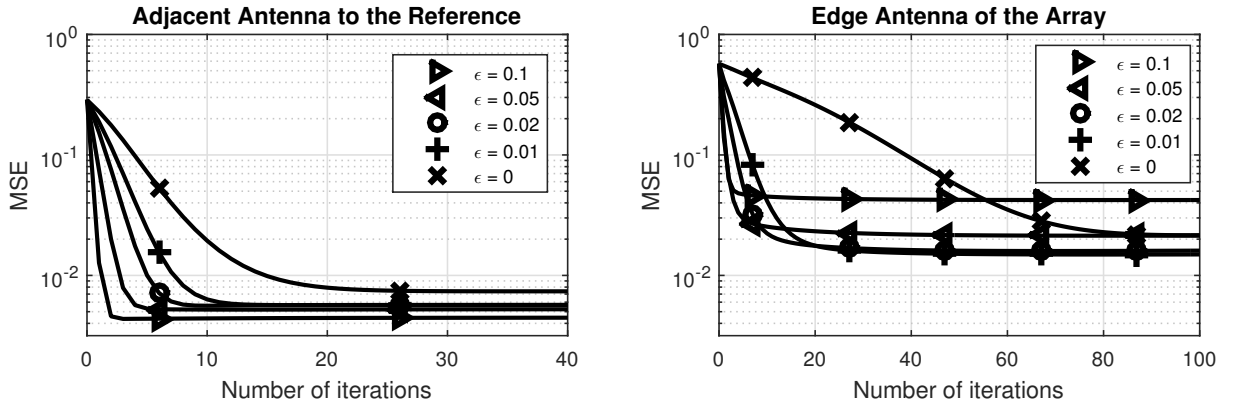


Fig. 4. MSE per iteration of the EM algorithm, for different regularization constants  $\epsilon$ . This plots are for  $N_0 = 40$  dB, and the remaining simulation settings are the same as Fig. 3. Note the different scales of the independent variable in the plots.

## V. VALIDATION OF THE CALIBRATION METHOD IN A MASSIVE MIMO TESTBED

For validation we implemented the proposed calibration method in a software-defined radio based massive MIMO testbed, and performed a TDD transmission from 100 BS antennas to 3 closely spaced single antenna users. Detailed information on the testbed can be found in [23].

The analysis conducted in this section and in Sec. VI is predominantly measurement based, with data obtained from the testbed described next. As this required stationarity of the processes being measured, we monitored the system temperature throughout the measurements and no significant variations were registered.

### A. Brief Information about the Testbed

1) *Antenna/Transceiver setup*: Semi-rigid SMA cables link the 100 BS antenna ports to the antenna ports of 50 software-defined radios (SDRs), where each SDR has two RF analog front-ends. For simplicity, the same transceiver settings, e.g. transmit power amplifier (PA) gain and receive automatic gain control (AGC), are used in both calibration and data communication stages for all radio units. This ensures that the RF front-ends yield the same response during both stages, thus

the calibration is valid during the data transmission stage.<sup>8</sup>

2) *Time and Frequency synchronization of the radios*: Frequency synchronization is achieved by distributing a reference signal generated by a crystal-oven oscillator to all radio units. However, this does not guarantee phase alignment between all BS transceiver radio chains which motivates reciprocity calibration. We note that, under stable temperature conditions, the calibration is valid for a very large amount of time, due to the low time-varying response of the analog components [23]. Time synchronization is achieved by another cable based network, which distributes synchronization signals to all radios.

### B. Signaling Protocol used

Once the measurements to construct the observation matrix  $\mathbf{Y}$  are performed, the calibration coefficients  $c_m$  are estimated using the EM algorithm. The following sequence of events are then performed periodically:

1) *Uplink Channel Estimation and Calibration*: Users simultaneously transmit frequency orthogonal pilot symbols. The BS performs LS-based channel estimation, and interpolates the estimates between pilot symbols. Reciprocity cali-

<sup>8</sup>However, it was verified during our experiments that no noticeable performance degradation occurred if the PAs and AGCs operate during the data transmission stage with gains say, 10 dB away from the gains setting used during calibration. We leave this matter for future investigation.

TABLE I  
HIGH-LEVEL OFDM PARAMETERS USED

Parameter	Variable	Value
Bandwidth	$W$	5 MHz
Carrier frequency	$f_c$	3.7 GHz
Sampling Rate	$F_s$	7.68 MS/s
FFT Size	$N_{\text{FFT}}$	2048
# Used sub-carriers	$N_{\text{SUB}}$	1200

bration is then performed independently per subcarrier, i.e. as in (3), for coherence purposes with Sec. II.<sup>9</sup> This calibrated version of the downlink channel is then used to construct a ZF precoder.

#### 2) Downlink channel estimation and data transmission:

Downlink pilot symbols are precoded in the downlink and each user performs LS-based channel estimation. Using the estimates, each user recovers the payload data using a one-tap equalizer.

We note that 4-QAM signaling per OFDM sub-carrier was used for uplink channel estimation and data transmission. The main parameters are shown in Table I. Further information on the signaling protocol used, e.g. uplink/downlink frame structure or uplink pilot design, is found on [23].

### C. Measurement Description

The experimental setup used is shown in Figure 1. Although not being a typical propagation scenario found in cellular systems, this extreme setup - closely located users under strong line-of-sight conditions - requires high calibration requirements to be met if spatial separation of users is to be achieved. We use this setup in our experiments for validation purposes. In addition, we use ZF precoding since it is known to be very sensitive to calibration errors [22].

We made an effort to keep static propagation conditions during the measurements session, and thus performed the measurements at late hours in our lab when no people were around.

The EVM [29] of the downlink equalized received samples at each mobile station was evaluated, and used as performance metric for validation purposes. The rationale is that, with multiple mobile terminals, calibration errors translate into downlink inter-user interference and loss of array gain, which degrades the EVM. Letting  $r$  be the downlink equalized received sample when symbol  $s$  is transmitted, the EVM is defined as

$$\text{EVM} = \text{E} \left\{ \frac{|r - s|^2}{|s|^2} \right\}, \quad (33)$$

where the expectation is taken over all system noise sources, e.g., hardware impairments and thermal noise. Our estimate of (33) was obtained by averaging realizations of  $|r - s|^2/|s|^2$  over all OFDM sub-carriers and over received OFDM symbols.

We estimated the EVM for different energy values of the uplink pilots and calibration signals. We do so in order to be able to extract insightful remarks for the analysis of the results. In particular, letting  $E_{\text{Pilot}} = \text{E} \{p_k p_k^*\}$  in (1) denote

the energy of the uplink pilot, which, for simplicity, is the same for all users, and let  $E_{\text{Cal}}$  denote the energy of the sounding signal  $s_m$  in (5), we estimated the EVM for a 2-dimensional grid of  $E_{\text{Pilot}}$  and  $E_{\text{Cal}}$ . The results reported next are given with respect to the relative energies  $Er_{\text{Pilot}} = E_{\text{Pilot}}/E_{\text{Pilot}}^{\text{max}}$  and  $Er_{\text{Cal}} = E_{\text{Cal}}/E_{\text{Cal}}^{\text{max}}$ , where  $E_{\text{Pilot}}^{\text{max}}$  and  $E_{\text{Cal}}^{\text{max}}$  are the maximum energies of the uplink pilot and calibration signal used in the experiments. Other systems parameters - e.g. transmit power in the downlink - were empirically set and kept constant throughout the experiment.

### D. Validation Results

Fig. 5 shows the measured EVMs in decibel, for the three user stations in our experiment. Before discussing the results, we remark that analyzing the EVM when  $Er_{\text{Cal}}$  is reduced beyond  $-30$  dB is not of fundamental interest, as it approaches the uncalibrated case where high EVMs are to be expected. Overall, a positive trend is observed with increasing  $Er_{\text{Cal}}$  until  $-10$  dB. This reflects the BS ability of spatially separating users which increases with increasing the calibration quality. The fact that downlink EVMs down to  $-10$  dB are achieved, which are much smaller than the EVMs achieved for  $Er_{\text{Cal}} = -30$  dB, i.e. close to the uncalibrated case, motivates our validation claim.

It is possible to observe a saturation of the EVMs at high enough  $Er_{\text{Cal}}$  and  $Er_{\text{Pilot}}$  values. This is, however, an expected effect in practical systems. In short, system impairments other than the calibration or the uplink channel estimation error, become the main elements that constrain the EVM performance. For example, the presence of measurement noise at the user stations when a constant downlink power is used. Remarkably, this saturation effect implies that the calibration SNR - available in a practical array as ours - is sufficiently large not to be the main impairment to constrain the system performance. The mutual coupling channels are thus reliable and reciprocal enough, so that they can be used for signaling in order to calibrate the array.

## VI. ASPECTS OF WIDEBAND CALIBRATION AND ERROR MODELING

A short summary of the section follows. We treat the calibration coefficient estimates - obtained with the EM algorithm - across OFDM sub-carriers as a discrete stochastic process. Using low rank approximation theory, we propose a parametrized low dimensional basis that characterizes the subspace spanned by this process well. Based on the reduced basis, we propose a wideband estimator that averages out the calibration error across the sub-carriers. To finalize, we provide a statistical model for the calibration error. We remark that our experiment makes use of a bandwidth of  $F_s N_{\text{sub}}/N_{\text{FFT}} = 4.5$  MHz.

### A. Wideband Remarks for the Calibration Coefficients

Denote the calibration coefficient of BS antenna  $m$  at the  $k$ th OFDM sub-carrier as  $C_m[k] = t_m^k/r_m^k$ . The variable  $\hat{C}_m[k]$  is the estimate of  $C_m[k]$  at sub-carrier  $k$  - obtained,

<sup>9</sup>We address wideband calibration in Sec. VI.

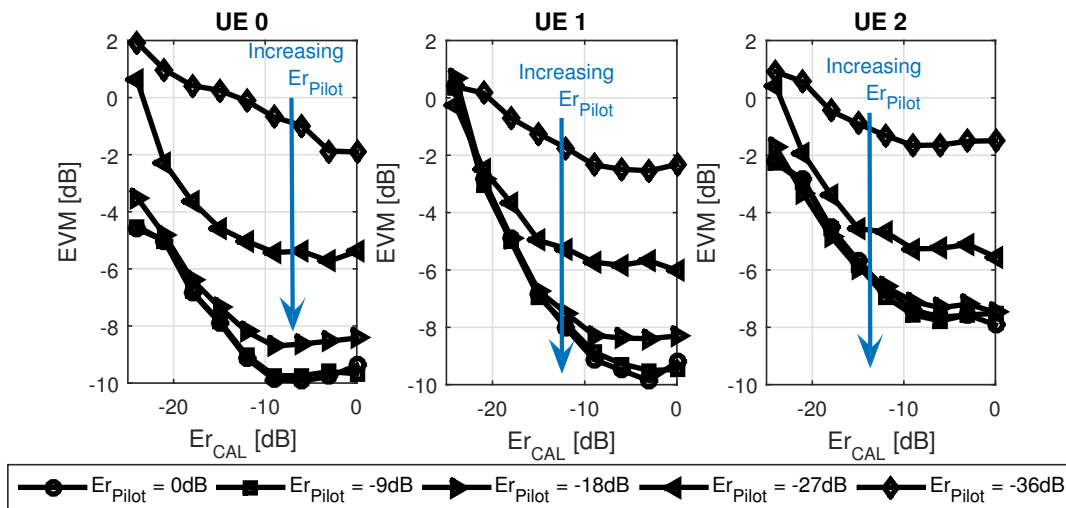


Fig. 5. Measured EVM at each of the three user stations during a massive MIMO downlink transmission.

e.g., with the EM algorithm - and is modeled as

$$\begin{aligned}\hat{C}_m[k] &= C_m[k] + E_m[k] \\ &= |C_m[k]| \exp(j2\pi\zeta_m[k]) + E_m[k]\end{aligned}\quad (34)$$

where  $E_m[k]$  is an i.i.d. random process representing the calibration error which is assumed zero-mean and independent of  $C_m[k]$ .

Let the random phasor process  $\exp(j2\pi\zeta_m[k])$  in (34) absorb the phase shift stemming from the arbitrary time that a local oscillator needs to lock to a reference signal. Such phase shift is often modeled as uniformly distributed, and thus

$$E\{\exp(j2\pi\zeta_m[k])\} = 0. \quad (35)$$

Moreover, since local oscillators associated with different transceivers lock at arbitrary times, it is safe to assume

$$E\{\exp(j2\pi\zeta_m[k_1]) \exp(-j2\pi\zeta_n[k_2])\} = 0, \quad m \neq n. \quad (36)$$

Not making further assumptions on the statistics of  $\hat{C}_m[k]$ , we now proceed with a series expansion, but before doing so we make one last remark.

The series expansion conducted next is performed based on measurements from the 100 testbed transceivers, and serves as an example approach to obtain a suitable basis for  $\hat{C}_m[k]$ . This can well apply to mass-production transceiver manufactures that can reliably estimate the statistical properties of the hardware produced. However, as our testbed operates with relatively high-end transceivers - compared to the ones expected to integrate commercial massive MIMO BSs - the dimensionality of the subspace verified in our analysis might be underestimated. Intuitively, the higher transceiver quality, the less basis functions are needed to accurately describe  $\hat{C}_m[k]$ . Nevertheless, the upcoming remarks apply for arbitrary smaller bandwidths - than 4.5MHz - depending on the hardware properties of the transceivers.

### B. Principal Component Analysis

Given that  $\hat{C}_m[k]$  is a zero-mean discrete process, the element at the  $v_1$ th row and  $v_2$ th column of its covariance

matrix  $\mathbf{K}_m$  is defined as

$$[\mathbf{K}_m]_{[v_1, v_2]} = E\{\hat{C}_m[v_1] \hat{C}_m^*[v_2]\}. \quad (37)$$

Due to the property in (36), the principal components of  $\hat{C}_m[k]$  are obtained by singular value decomposition (SVD) of  $\mathbf{K}_m$  only [30]. Let the SVD of  $\mathbf{K}_m$  be written as

$$\mathbf{K}_m = \sum_{i=1}^{N_{\text{SUB}}} \mathbf{u}_i^m \lambda_i^m (\mathbf{u}_i^m)^H, \quad (38)$$

where  $\{\mathbf{u}_i^m\}_{i=1}^{N_{\text{SUB}}}$  are the principal components, and  $\lambda_i^m$  is the power (variance) of the coefficient obtained from projecting  $\hat{C}_m[k]$  into  $\mathbf{u}_i^m$ . We use the convention  $\lambda_1^m \geq \lambda_2^m \geq \dots \geq \lambda_{N_{\text{SUB}}}^m$ , and  $\mathbf{u}_i^m = [[u_i^m[1], \dots, u_i^m[N_{\text{SUB}}]]^T$ . Fig. 6 shows several coefficients and basis functions of the expansion, that were estimated based on 100 realizations of  $\hat{C}_m[k]$ , each measured with  $Er_{\text{CAL}} = 5$  dB, which from Fig. 5, provides a relatively high calibration SNR. Noticeably, it appears that all processes, i.e. one per transceiver, live mostly in a one-dimensional sub-space and thus can be well described by their first principal component  $\mathbf{u}_1^m$ . This fact also indicates that the contribution of the calibration error in the expansion is small, and thus the basis found for  $\hat{C}_m[k]$  is also representative for the true coefficients  $C_m[k]$ .

Visual inspection indicates that both magnitude and phase of the first principal component can be well approximated with a linear slope across frequency. The inherent error of this approximation is very small compared to the magnitude of the process itself. We note that this linear trend holds for any transceiver of the array (not only for the ones in Fig. 6).

### C. Wideband Modeling and Estimation

The previous analysis indicates that any first principal component can be well described by a linear magnitude slope  $\gamma_m$ , and a linear phase slope  $\phi_m$  across frequency. Such properties are well captured by the Laplace kernel

$$\exp((\gamma_m + j2\pi\phi_m)k),$$

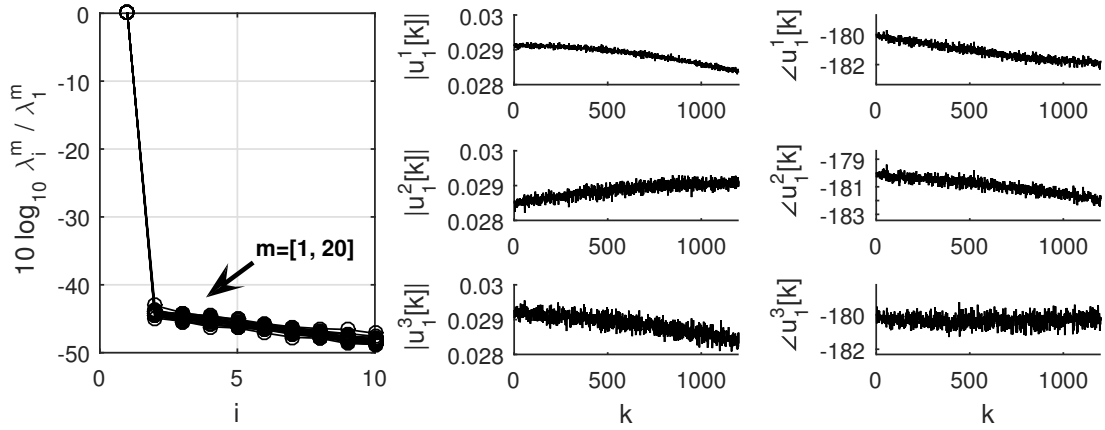


Fig. 6. Principal component and coefficients of  $\hat{C}_m[k]$ . *Left*) The 10 strongest normalized singular values of the expansion for 20 transceivers; *Middle*) Magnitude of the first principal component for 3 different transceivers; *Right*) Phase of the first principal component for 3 different transceivers.

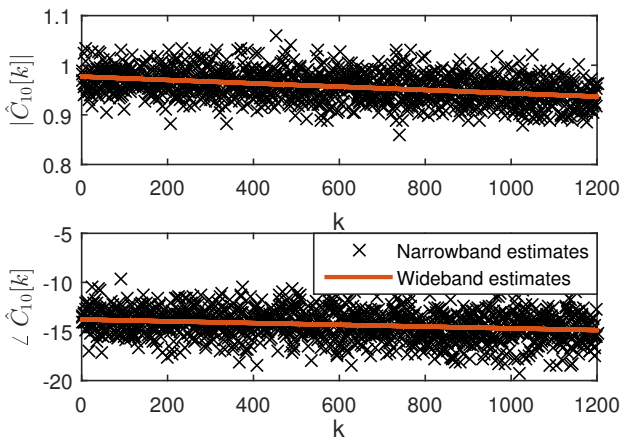


Fig. 7. A realization of the narrow-band estimator  $\hat{C}_m[k]$ , and the proposed wideband estimator  $\hat{C}_i[k]^{\text{WB}}$ .

for small values of  $|\gamma_m|$ . The final parameter to model a realization of the process is the complex offset  $A_m$ . With that, the general model (34) can thus be re-written as

$$\hat{C}_m[k] = A_m \exp((\gamma_m + j2\pi\phi_m)k) + w_m[k], \quad (39)$$

where  $w_m[k]$  is a random process that absorbs the calibration error  $E_m[k]$ , the error due to the low rank approximation, and the error due to the linear modeling of the first principal component  $\mathbf{u}_1^m$ . Given an observation  $\{\hat{C}_m[k]\}_{k=1}^{N_{\text{SUB}}}$ , the ML estimate of  $A_m$ ,  $\phi_m$  and  $\gamma_m$ , namely,  $\hat{A}_m$ ,  $\hat{\phi}_m$  and  $\hat{\gamma}_m$  is straightforward to derive [27]. Thus, we define the wideband estimator of  $\hat{C}_m[k]$  as

$$\hat{C}_m[k]^{\text{WB}} = \hat{A}_m \exp((\hat{\gamma}_m + j2\pi\hat{\phi}_m)k). \quad (40)$$

For illustration purposes, a realization for the ML wideband estimator  $\hat{C}_m[k]^{\text{WB}}$  is contrasted with that of the narrow-band calibration coefficients  $\hat{C}_m[k]$  in Fig. 7. The error reduction obtained by exploiting the structure of the process is evident.

#### D. A Model for the Calibration Error

Here we verify that the calibration error produced by a narrow-band estimator, e.g. the EM algorithm, is Gaussian.

This is performed under two main assumptions detailed next.

1) *The residual process  $E_m[k] = \hat{C}_m[k] - C_m[k]$  is well described by  $\hat{E}_m[k] = \hat{C}_m[k] - \hat{C}_m[k]^{\text{WB}}$ .* This is reasonable if  $\mathbb{E}\{|\hat{C}_m[k]^{\text{WB}} - C_m[k]|^2\} \ll \mathbb{E}\{|\hat{C}_m[k] - C_m[k]|^2\}$ . To justify, the gains due to averaging are known to be linear in the number of realizations [27], which is  $N_{\text{SUB}} = 1200$  in this case. If the estimation error is independent across realizations, the underlying model (39) models the first principal component well, and the error due to low rank approximation is minuscule, there are potential gains of  $10 \log_{10} N_{\text{SUB}} \approx 30$  dB.

2) *The residual process  $E_m[k]$  is ergodic.*<sup>10</sup> This is met if  $E_m[k]$  is stationary and the ensemble of  $N_{\text{SUB}}$  samples is representative enough for statistical modeling. The former can be assumed for sufficiently small OFDM bandwidths so that the hardware impairments do not vary significantly across sub-carriers. The latter is also met, as we have  $N_{\text{SUB}} = 1200$  narrow-band estimators whose estimated errors  $\{\hat{E}_m[k]\}_{k=1}^{N_{\text{SUB}}}$  were found to be mutually uncorrelated.

Fig. 8 shows the empirical cumulative distribution function (CDF) of both real and imaginary parts of  $\{\hat{E}_m[k]\}_{k=1}^{N_{\text{SUB}}}$  - which we found to be uncorrelated - for two transceiver cases. Each of the empirical CDFs is contrasted with a zero-mean Gaussian distribution of equal variance. Overall, the empirical CDFs for both transceivers resemble a Gaussian CDF extremely well. The Gaussianity of the calibration error was further verified by passing a Kolmogorov-Smirnov test with 0.05 significance level [31]. We note that these observations hold not only for the two transceivers in Fig. 8, but for all transceivers of the array.

Noticeably, the empirical distribution of the calibration error is in line with the high SNR asymptotic properties of ML estimators, i.e. the error can be modeled by an additive zero-mean Gaussian random variable. The final element left for a full characterization is its covariance matrix, which relates eventual correlations across antennas. A good approximation

<sup>10</sup>Ergodicity is necessary since each (independent) measurement of  $\hat{C}_m[k]$  takes about ten minutes with our test system. As potential system temperature drifts during the assemblment can result in varying statistical properties, it is safer to perform the analysis based on one solely realization of  $E_m[k]$ .

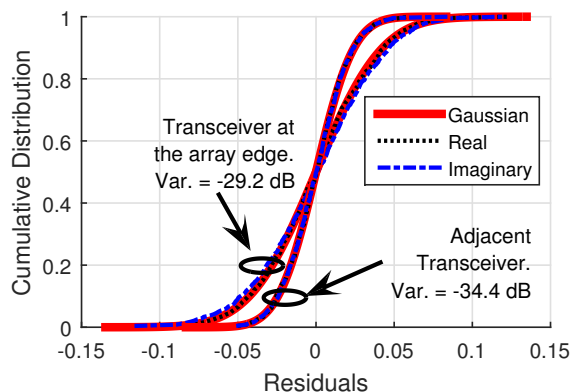


Fig. 8. Empirical CDFs for the real and imaginary parts of the calibration error, for a transceiver at the edge of the array, and for an adjacent transceiver to the reference antenna. A Gaussian CDF of equal variance is plotted for both cases for comparison.

is the inverse of the transformed Fisher Information matrix in (27). Noticeably, future calibration works can benefit from the convenience of safely assuming a Gaussian calibration error.

## VII. CONCLUSIONS

We have proposed and validated a convenient calibration method, which rely on mutual coupling - an often unwanted property of antenna arrays - to re-establish the reciprocity assumption in TDD massive MIMO systems. We verified that in a practical antenna array, the channels due to mutual coupling are reliable and reciprocal enough, so that they can be used for signaling.

The EM-algorithm proposed for calibration is asymptotically efficient and outperforms current state-of-the-art estimators in an MSE sense. The computational complexity is reduced compared to previous schemes, and convergence can be attained within a few iterations. The calibration error can be further reduced by proper averaging over the radio bandwidth, and from our experiments, it did not stand as the main impairment to constraint the performance of the system.

Our measurements verify that the calibration error is Gaussian distributed, which is coherent with the theory of the estimator used. The convenience of safely assuming a Gaussian calibration error can aid the analysis of TDD massive MIMO systems in future works.

## ACKNOWLEDGMENTS

This work was funded by the Swedish foundation for strategic research SSF, VR, the strategic research area ELLIIT, and the E.U. Seventh Framework Programme (FP7/2007-2013) under grant agreement n 619086 (MAMMOET). We also thank the Comm. Systems group in Bristol University, for letting us replicate several of our results in their testbed.

## REFERENCES

- [1] F. Rusek, D. Persson, B. K. Lau, E. G. Larsson, T. L. Marzetta, O. Edfors, and F. Tufvesson, "Scaling up MIMO: opportunities and challenges with very large arrays," *IEEE Signal Processing Magazine*, vol. 30, no. 1, pp. 40–60, 2013.
- [2] E. G. Larsson, O. Edfors, F. Tufvesson, and T. L. Marzetta, "Massive MIMO for next generation wireless systems," *IEEE Communications Magazine*, vol. 52, no. 2, pp. 186–195, 2014.

- [3] L. Zheng and D. N. C. Tse, "Communication on the Grassmann manifold: a geometric approach to the noncoherent multiple-antenna channel," *IEEE Transactions on Information Theory*, vol. 48, no. 2, pp. 359–383, Feb 2002.
- [4] T. L. Marzetta, "Noncooperative cellular wireless with unlimited numbers of base station antennas," *Trans. Wireless. Comm.*, vol. 9, no. 11, pp. 3590–3600, Nov. 2010.
- [5] M. Salehi and J. Proakis, *Digital Communications*. McGraw-Hill Education, 2007.
- [6] C. A. Balanis, *Antenna Theory: Analysis and Design*. Wiley-Interscience, 2005.
- [7] F. Kaltenberger, H. Jiang, M. Guillaud, and R. Knopp, "Relative channel reciprocity calibration in MIMO/TDD systems," in *Future Network and Mobile Summit, 2010*, June 2010.
- [8] M. Petermann, M. Stefer, F. Ludwig, D. Wubben, M. Schneider, S. Paul, and K.-D. Kammeyer, "Multi-User Pre-Processing in Multi-Antenna OFDM TDD Systems with Non-Reciprocal Transceivers," *Communications, IEEE Transactions on*, vol. 61, no. 9, pp. 3781–3793, September 2013.
- [9] A. Bourdoux, B. Come, and N. Khaled, "Non-reciprocal transceivers in OFDM/SDMA systems: impact and mitigation," in *Radio and Wireless Conference, 2003. RAWCON '03. Proceedings*, Aug 2003, pp. 183–186.
- [10] K. Nishimori, K. Cho, Y. Takatori, and T. Hori, "Automatic calibration method using transmitting signals of an adaptive array for TDD systems," *IEEE Transactions on Vehicular Technology*, vol. 50, no. 6, pp. 1636–1640, Nov 2001.
- [11] K. Nishimori, T. Hiraguri, T. Ogawa, and H. Yamada, "Effectiveness of implicit beamforming using calibration technique in massive MIMO system," in *Electromagnetics (iWEM), 2014 IEEE International Workshop on*, Aug 2014, pp. 117–118.
- [12] X. Luo, "Robust Large Scale Calibration for Massive MIMO," in *2015 IEEE Global Communications Conference (GLOBECOM)*, Dec 2015.
- [13] H. Wei, D. Wang, H. Zhu, J. Wang, S. Sun, and X. You, "Mutual Coupling Calibration for Multiuser Massive MIMO Systems," *IEEE Transactions on Wireless Communications*, vol. 15, no. 1, pp. 606–619, Jan 2016.
- [14] R. Rogalin, O. Bursalioglu, H. Papadopoulos, G. Caire, A. Molisch, A. Michaloliakos, V. Balan, and K. Psounis, "Scalable Synchronization and Reciprocity Calibration for Distributed Multiuser MIMO," *Wireless Communications, IEEE Transactions on*, vol. 13, no. 4, April 2014.
- [15] C. Shepard, H. Yu, N. Anand, E. Li, T. Marzetta, R. Yang, and L. Zhong, "Argos: Practical many-antenna base stations," in *Proceedings of the 18th Annual International Conference on Mobile Computing and Networking*, ser. Mobicom '12. New York, NY, USA: ACM, 2012, pp. 53–64.
- [16] P. Zetterberg, "Experimental Investigation of TDD Reciprocity-based Zero-forcing Transmit Precoding," *EURASIP J. Adv. Signal Process*, vol. 2011, pp. 5:1–5:10, Jan. 2011.
- [17] R. Rogalin, O. Y. Bursalioglu, H. C. Papadopoulos, G. Caire, and A. F. Molisch, "Hardware-impairment compensation for enabling distributed large-scale mimo," in *Information Theory and Applications Workshop (ITA), 2013*, Feb 2013.
- [18] H. Papadopoulos, O. Bursalioglu, and G. Caire, "Avalanche: Fast RF calibration of massive arrays," in *Signal and Information Processing (GlobalSIP), 2014 IEEE Global Conference on*, Dec 2014, pp. 607–611.
- [19] J. Vieira, F. Rusek, and F. Tufvesson, "Reciprocity calibration methods for massive MIMO based on antenna coupling," in *Global Communications Conference (GLOBECOM), 2014 IEEE*, Dec 2014, pp. 3708–3712.
- [20] H. Wei, D. Wang, and X. You, "Reciprocity of mutual coupling for TDD massive MIMO systems," in *Wireless Communications Signal Processing (WCSP), 2015 International Conference on*, Oct 2015.
- [21] X. Jiang, M. Cirkic, F. Kaltenberger, E. G. Larsson, L. Deneire, and R. Knopp, "MIMO-TDD reciprocity under hardware imbalances: Experimental results," in *ICC 2015, IEEE International Conference on Communications, 8-12 June 2015, London, United Kingdom*, London, U.K., 2015.
- [22] W. Zhang, H. Ren, C. Pan, M. Chen, R. C. de Lamare, B. Du, and J. Dai, "Large-Scale Antenna Systems With UL/DL Hardware Mismatch: Achievable Rates Analysis and Calibration," *IEEE Transactions on Communications*, vol. 63, no. 4, pp. 1216–1229, April 2015.
- [23] J. Vieira, S. Malkowsky, K. Nieman, Z. Miers, N. Kundargi, L. Liu, I. Wong and V. Öwall and O. Edfors and F. Tufvesson, "A flexible 100-antenna testbed for Massive MIMO," in *IEEE GLOBECOM 2014 Workshop on Massive MIMO: from theory to practice*, Dec 2014.
- [24] R. Jedlicka, M. Poe, and K. Carver, "Measured mutual coupling between microstrip antennas," *Antennas and Propagation, IEEE Transactions on*, vol. 29, no. 1, pp. 147–149, Jan 1981.

- [25] A. Hall, *Generalized Method of Moments*, ser. Advanced Texts in Econometrics. OUP Oxford, 2004.
- [26] V. Mehrmann and H. Voss, "Nonlinear eigenvalue problems: a challenge for modern eigenvalue methods," *GAMM-Mitteilungen*, vol. 27, no. 2, pp. 121–152, 2004.
- [27] S. M. Kay, *Fundamentals of Statistical Signal Processing: Estimation Theory*. Upper Saddle River, NJ, USA: Prentice-Hall, Inc., 1993.
- [28] A. Molisch, *Wireless Communications*, ser. Wiley - IEEE. Wiley, 2010.
- [29] T. Schenk, *RF Imperfections in High-rate Wireless Systems: Impact and Digital Compensation*. Springer Netherlands, 2008.
- [30] H. Van Trees, *Detection, Estimation, and Modulation Theory*, ser. Detection, Estimation, and Modulation Theory. Wiley, 2004.
- [31] W. Daniel, *Applied nonparametric statistics*, ser. The Duxbury advanced series in statistics and decision sciences. PWS-Kent Publ., 1990.